Self-Mixing Interferometry on Long Distance: Theory and Experimental Validation

Alfred Albert, Silvano Donati, *Life Fellow, IEEE*, and San-Liang Lee, *Senior Member, IEEE*

***Abstract*— We consider the operation of a self-mixing interferometer on distances larger than the laboratory scale, that is, tens to hundreds of meters, and develop for the first time the theoretical analysis of SMI performances in the near and far field (FF), presenting results about signal amplitude (AM), SNR, C factor, spot size, and linewidth. Theory is also valid for the realistic case of an elliptical laser spot. Thereafter, we compare the theoretical findings with experimental data measured on white paper target using a diode laser SMI operating at 1550 nm, with a SNR = 3.6 at 12-m distance and find good agreement. These results open the way to long stand-off vibration, displacement, and distance/velocity measurements.**

***Index Terms*— Interferometry, optical feedback, optical measurements, semiconductor lasers.**

I. Introduction

THE Self-mixing interferometry (SMI) is a well-known coherent technique for measuring a number of physical quantities—in particular kinematics, such as displacements, vibrations, distance, and velocity [1], [2], [3], [4], and is especially attractive because of its simple and compact setup and the ease of operation.

Indeed, in the self-mixing basic scheme (Fig. 1), there is no need for an optical interferometer external to the laser source, and the cosine and sine of the optical pathlength 2kD ($k = 2\pi/\lambda$) being the wavevector and D the distance to the target under measurement (kD) are obtained from the interaction of the optical field fed back into the laser cavity. This interaction generates amplitude modulation (AM) and frequency modulation (FM) whose indexes are just the cosine and sine signals provided by the optical interferometer of the conventional scheme. The AM signal is readily picked by detecting the emitted laser power and we can use the rear mirror output (as in Fig. 1) to get the cosine signal due to the monitor photodiode commonly mounted by the manufacturer in the same package with the diode laser chip, whereas the FM signal is more difficult to retrieve [5] and is less frequently used.

The AM power signal P_{SMI}, converted into an output current I_{PD} by the photodiode with spectral sensitivity σ_{PD}, is written as [1], [2], [3]

$$I_{\mathrm{PD}} = \sigma_{\mathrm{PD}} P_{\mathrm{SMI}} = \sigma_{\mathrm{PD}} P_0 (1 + m \cos 2\mathrm{kD}) \tag{1}$$

where P_{SMI} is the power exiting from the rear mirror and reaching the photodiode (Fig. 1), given by the sum of the unperturbed component P_0 normally supplied by the laser and of the self-mixing contribution P_0m cos 2kD; m is the AM modulation index found as [1], [3], [5]

$$m = 2(\tau_p/\tau_{\mathrm{in}})\eta_E \eta_m (1 - r_2^2)/\mathrm{G}r_2 \tag{2}$$

where τ_p (typ. 5, . . . , 10 ps) and τ_{in}(typ. 10, . . . , 20 ps) are the photon lifetime and the cavity roundtrip time of the laser, respectively, r_2(typ. 0.55) is the field reflectivity of the laser front mirror, η_m (typ. 0.5) is the mode superposition factor [1], [2], [3], [4], [28], G ≈ 1 is the gain minus loss experienced by P_{back} crossing the laser and exiting from the rear mirror [6], and

$$\eta_E = \sqrt{\eta_p} = \sqrt{(P_{\mathrm{back}}/P_{\mathrm{out}})} \tag{3}$$

is the field feedback factor, square root of the power feedback factor η_p defined on its turn as the ratio of power P_{back} returning from the target into the laser to the power P_{out} out of the objective lens (Fig. 1).

With the typical values quoted above, (2) gives

$$m = 0.6\ \eta_E. \tag{4}$$

Moreover, from (1) to (2), we see that the useful self-mixing interferometer (SMI) current signal $I_{\mathrm{SMI}} = \sigma_{\mathrm{PD}} P_0$m cos 2kD is proportional to η_E, the key quantity of the SMI measurement, that we will calculate as a function of distance D in the next section.

Factor η_E is important because: 1) it tells us that the detected signal is proportional to the square root of power $\sqrt{P_{\mathrm{back}}} \propto E_{\mathrm{back}}$, i.e., proportional to the field E_{back}, thus indicating that the self-mixing is a coherent process, and as such, it works at the quantum limit of detection [7] and 2) because it determines both the signal AM $\eta_E I_0$ and the ultimate measurement SNR at the quantum limit [1], [3], readily written as $\mathrm{SNR}_{\mathrm{q.l.}} = \eta_E I_0/\sqrt{(2\mathrm{e}I_0\mathrm{B})} = \eta_E[I_0/(2\mathrm{eB})]^{1/2}$, where we have let the shot noise of current $I_0 = \sigma_{\mathrm{PD}} P_0$ as $\sqrt{(2\mathrm{e}I_0\mathrm{B})}$ [7].

Another important parameter of the SMI is the C-factor, also known as Acket factor or feedback parameter [1], [2], [3]

$$\mathrm{C} = \sqrt{(1 + \alpha^2)}(\tau_{\mathrm{ext}}/\tau_{\mathrm{in}})\eta_E \eta_m (1 - r_2^2)/r_2 \tag{5}$$

Received 20 June 2024; revised 14 September 2024; accepted 26 September 2024. Date of publication 23 October 2024; date of current version 5 November 2024. This work was supported by the Ministry of Science and Technology, Taiwan, under NSTC under Project 112-2221-E-011-03-MY3. The Associate Editor coordinating the review process was Dr. Ernst Csencsics. *(Corresponding author: Silvano Donati.)*

Alfred Albert is with the Department of Electronic and Computer Engineering, National Taiwan University of Science and Technology, Taipei 106335, Taiwan.

Silvano Donati is with the Department of Industrial Engineering and Informatics, University of Pavia, 27100 Pavia, Italy, and also with HiSiPIC, Taipei 106335, Taiwan (e-mail: silvano.donati@unipv.it).

San-Liang Lee is with the Department of Electronic and Computer Engineering and the Heterogeneously-Integrated Silicon Photonic Integration Center (HiSiPIC), National Taiwan University of Science and Technology, Taipei 106335, Taiwan.

Digital Object Identifier 10.1109/TIM.2024.3485399

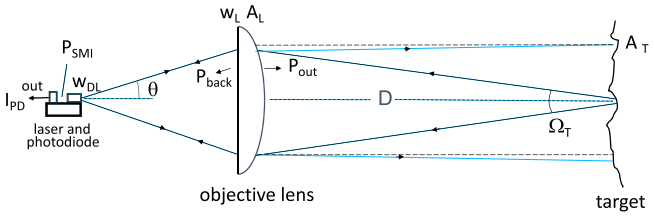

Fig. 1. Schematic of the SMI arrangement: light from the laser diode is collimated by an objective lens—power $P_{\text{out}-}$ onto a target area A_T at distance D. Light diffused back to the objective is focused into the laser cavity—power $P_{\text{back}-}$ and mixes with the unperturbed oscillation—acting as a local oscillator—on a photodiode at the rear facet, generating the output signal I_{PD}.

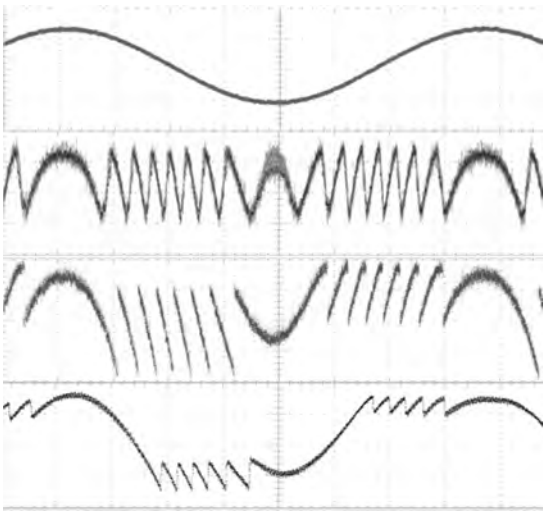

Fig. 2. Exemplary SMI waveforms illustrative of different C-factors. From top to bottom: the drive of target displacement, and the SMI waveforms. At $C = 0.5$, the waveform is distorted with one semi-period faster than the other; at $C = 1.5$, the waveform exhibits fast switching, and at $C = 4.5$, the waveform is very distorted. Vertical scale: 100 mV/div and horizontal scale 10 ms/div.

where α is the linewidth enhancement factor, also called Henry's parameter [1], [2], [3], [8], which describes the extra frequency noise due to the AM-to-frequency conversion of AM noise, $\tau_{\text{ext}} = 2\text{-D/c}$ is the roundtrip delay time to the target and back, and $\tau_{\text{in}} = 2n_c l_c/\text{c}$ is the roundtrip time in the laser cavity, long l_c, and or refraction index n_c.

The C factor is indicative of the feedback level and dramatically affects the waveform of the SMI signal (Fig. 2). At small C (e.g., <0.2, weak feedback), the waveform is an undistorted sine wave resembling that of a normal interferometer. But, starting at $\text{C} > 0.2$ and till $\text{C} < 1$ (medium feedback), the waveform is progressively distorted with the trailing edge becoming faster than the leading edge. When C reaches 1, the waveform exhibits a fast switching corresponding to a jump on the next external cavity mode [1], [2], [3], [4]. The regime continues, with a single switching per period in the range $1 < \text{C} < 4.6$ (medium to strong feedback), and then, we find double, triple, and so on switching per period for $\text{C} > 4.6$ [1], [2], [3]. At $\text{C} = 15$ and above, the waveform becomes chaotic and we can use it for optical cryptography [9], [10] but clearly not for measurement applications, for which the useful range should be limited to $\text{C} < 4.6$.

More information on SMI basic theory is provided by [3]; also, [2] is a nice tutorial on self-mix phenomena.

In applications, SMI is usually developed for the laboratory scale, with operation distances rarely in excess of, say, few tens of centimeters. One reason is because, in addition to the decreasing signal AM, at increasing distance, the waveform becomes distorted because of the large feedback factor and eventually might break into chaotic oscillations [10], [11].

In this article, for the first time, at the best of our knowledge, we present a thorough theoretical analysis of the measurement regime of SMI at long distances and calculate the expected signal AM, the SNR, the C-factor, and the linewidth (and associated coherence length) as a function of distance under feedback conditions.

Results show that even with moderate powers (mW), we can extend operation up to several tens of meters or even reach hundred meters on ordinary diffusing-surface targets and that long-cavity diode lasers are preferable for the less distorted waveform (lower C factor).

We also perform experimental measurements of waveforms taken with the SMI, both in the near field (NF) and the far field (FF), to check the validity of the theoretical results and find good agreement.

These results are useful in all applications of SMI and in particular for designing long stand-off distance vibrometers (i.e., sub-μm, periodic signal measurements) [4], displacement-measuring instruments (with fraction-of-λ resolution), and rangefinders (or LiDARs) for the 10- to 100-m range (with cm to dm resolution).

While the aim of the present work is not to develop any of these application in full details, we rather focus on important data for the validation of the above applications on the extended range of distance, analyzing maximum distance coverage with diffusing and retroreflecting targets, SNR, and spot size versus distance.

Previous work on long distance measurements and/or obstacle detection includes the development of a coherent detection integrated silicon photonics chip working up to 2 m [12], a feedback FMCW LiDAR based on an external cavity laser diode and a narrowband tuning crystal reaching 8.5 m [13], an SMI solid-state microchip-laser FMCW 3-D system with 65 m range [14], and a 10-m standoff distance diode-laser SMI vibrometer [15].

However, none of the above works reports any theoretical treatment of the quantities involved in the SMI measurement, like we develop in this article for the first time at the best of our knowledge.

This article is organized as follows. In Section II, we develop the theory of signal AM and associated parameters versus distance, in Section III, we present the measurements proving the correctness of the theory, in Section IV, we provide discussion and design hints, and finally, we draw conclusions.

II. Theory

Let us calculate the following quantities, which describe the SMI experiment on a distance D, as schematized in Fig. 1.

1) The power feedback factor $\eta_p = P_{\text{back}}/P_{\text{out}}$, fraction of power P_{back} returned by the target into the laser diode to the power P_{out} out of the objective lens, and the field feedback factor $\eta_E = E_{\text{back}}/E_{\text{out}} = \sqrt{\eta_p}$.

2) The signal AM $\sigma_{\rm PD} P_0 {\rm m} \cos 2{\rm kD}$.
3) The C factor of the SMI experiment.
4) The linewidth $\Delta\nu_{\rm SMI}$ under SMI operation and the associated coherence length $L_{\rm coh} = {\rm c}/\pi\Delta\nu_{\rm SMI}$ [16].
5) The spot size w_T at distance D.

In all the calculations, we start assuming a Lambertian (ideal) diffuser [7] as the target to satisfy the condition on noninvasiveness of the SMI in measurement application, and in the experimental validation, we use plain white paper as the diffusive target.

A. Feedback Factors

With reference to Fig. 1, we can calculate the power returning to the laser $P_{\rm back}$ as the product of the radiance R at the target times the backward acceptance [7] subtended by the objective lens, i.e., $A = A_T\Omega_T$, so that $P_{\rm back} = RA_T\Omega_T$.

Assuming lossless propagation, the total power exiting the objective lens $P_{\rm out}$ (Fig. 1), received by the target and by the target re-emitted in the semi-space in front of it is $P_{\rm out} = R\pi A_T$ (because the diffusing target emits on area A_T and a solid angle π for Lambert's law). We then multiply $P_{\rm back}$ by 1/2 to take account of the polarization randomization introduced by the diffusing target, as the laser chip is sensitive only to the component in the plane of the junction. Thus, the power feedback factor is given by

$$\eta_{\rm P} = P_{\rm back}/P_{\rm out} = 1/2(RA_T\Omega_T)/(R\pi A_T) = \Omega_T/2\pi. \quad (6)$$

About rays returning to the objective lens (Fig. 1), from the target at distance D, they are collected entirely by the laser when the angle of entrance, $\theta_{\rm back} = {\rm atan}\, w_L/{\rm D}$ ($w_{\rm L}$ being the lens radius), is smaller than the diffraction angle of the lens $\theta_{\rm diffr} = \lambda/\pi w_{\rm L}$ (i.e., $\theta_{\rm back} < \theta_{\rm diff}$), whereas for $\theta_{\rm back} > \theta_{\rm diffr}$, only rays fitting into the acceptance angle of the beam emitted by the laser ($\theta \le \theta_{\rm diff}$) are collected.

The two cases represent the FF and the NF of the propagation, and the solid angle of collection is, respectively

$$\Omega_{T-{\rm FF}} = \pi({w_{\rm L}}/{\rm D})^2 \text{ and } \Omega_{T-{\rm NF}} = \pi(\lambda/\pi w_L)^2. \quad (7)$$

The distance at which $\Omega_{T-{\rm FF}} = \Omega_{T-{\rm NF}}$ is the break-point between NF and FF and is known as the *Fresnel distance*; for a lens radius w_L, it is given by

$${\rm D}_F = \pi w_L^2/\lambda. \quad (8)$$

In applications, the lens radius value w_L shall be chosen to match the Gaussian spot size $w_{\rm G}$ of the beam reaching the lens surface by diffraction from the laser chip. As the power carried by a bidimensional Gaussian distribution [or Somb(r) function] within a radius $r = w_{\rm G}$ is 86% of the total power (see [3, Sec. A4.3]), $w_{\rm G}$ and w_L can also be made equal, and the residual 14% loss attributed is to the mode mismatch factor $\eta_{\rm m}$ of (2). If a more conservative choice $w_L = 2\ w_{\rm G}$(also called D4Σ) is preferred to achieve a $< 1\%$ loss, we still have $\eta_{\rm m} \approx 0.7$ because of the returning field distribution is nearly constant across the lens and is not well matched to the Gaussian of the laser. In the following, we assume for simplicity $w_{\rm G} = w_L$.

In the case of an elliptical spot size, D_F has two distinct values, $D_{F//} = \pi w_{\rm L//}^2/\lambda$ and $D_{F\perp} = \pi w_{\rm L\perp}^2/\lambda$, but it is convenient to resort to the equivalent circular-spot description (as discussed later in Section III-H) and use the geometrical mean of $D_{F//}$ and $D_{F\perp}$. With the value for our laser (see Section III-H), $w_{L//} = 0.75$ mm and $w_{L\perp} = 0.375$ mm, at $\lambda = 1.55\mu$m, we have

$${\rm D_{Feq}} = \pi w_{L//} w_{L\perp}/\lambda = 0.57 \text{ m}. \quad (9)$$

Worth to note, the ratio $[\Omega_{\rm TNF}/\Omega_{\rm T-FF}\ ]^{1/2} = \lambda {\rm D}/\pi {\rm w_L^2} = {\rm D}/{\rm D}_F$ is known as the *Fresnel number* N_F.

To find $\eta_{\rm P-FF}$, let us start considering the FF case in (1). By inserting in (6) $\Omega_T = \pi(w_L/{\rm D})^2$ for the FF, we have

$$\eta_{\rm P-FF} = 1/2(w_L/{\rm D})^2 \quad (10)$$

and the corresponding *field* feedback factor is

$$\eta_{E-{\rm FF}} = \sqrt{\eta_{\rm P-FF}} = 2^{-1/2} w_L/{\rm D}. \quad (11)$$

In the NF, at ${\rm D} < {\rm D}_F$, we multiply (8) by $\Omega_{\rm TNF}/\Omega_{T-{\rm FF}} = ({\rm D}/{\rm D}_F)^2$ and obtain the $\eta_{\rm P-NF}$ as

$$\eta_{\rm P-NF} = 1/2(w_L/{\rm D}_F)^2 \quad (12)$$

and the corresponding field attenuation is

$$\eta_{E-{\rm NF}} = \sqrt{\eta_{\rm P-NF}} = 2^{-1/2}(w_L/{\rm D}_F). \quad (13)$$

B. Signal AM

The SMI signal AM is given by the second term at the right-hand side of (1). Using (11) and (13), we get for the peak value (i.e., at $\cos 2{\rm kD} = 1$) of the signal current

$$I_{\rm PD-FF} = 0.425\ I_{\rm PD0}(w_L/{\rm D}), \text{ and} \quad (14)$$
$$I_{\rm PD-NF} = 0.425\ I_{\rm PD0}(w_L/{\rm D}_F). \quad (15)$$

Equations (14) and (15) tell us the SMI signal is constant in the NF and then decreases as 1/D in the FF, as confirmed experimentally (Section III-A).

For an elliptical spot, power and thus detected current $I_{\rm PD0}$ is shared equally in the two x- and y-axes of the spot distribution; by using (14) and (15), and being 0.212 the AM of each current component, we can write, in the FF and NF

$$\begin{aligned} I_{\rm PD-FF} &= 0.212\ I_{\rm PD0}\left(w_{L//} + w_{L\perp}\right)/{\rm D} = 0.425\ w_{\rm Leq}/{\rm D} \\ I_{\rm PD-NFt} &= 0.212\ I_{\rm PD0}\left(w_{L//}/{\rm D}_{F//} + w_{L\perp}/{\rm D}_{F\perp}\right) \\ &= 0.425\ I_{\rm PD0} w_{\rm Leq}/{\rm D_{Feq}} \end{aligned} \quad (16)$$

where we have let

$$w_{\rm Leq} = \left(w_{L//} + w_{L\perp}\right)/2 \text{ and } {\rm D_{Feq}} = \left[{\rm D}_{F\perp}{\rm D}_{F//}\right]^{1/2}. \quad (17)$$

Equation (17) tells us that $w_{\rm Leq}$ and $\rm D_{Feq}$ can be assumed as the circular-spot equivalent of beam size and Fresnel distance.

In the NF, the signal $I_{\rm PD}$ is constant and then rolls off in the FF as the inverse of distance. The break point is at the distance ${\rm D} = {\rm D_{Feq}}$, such that $(\lambda/\pi)(1/w_{L//} + 1/w_{L\perp}) = (w_{L//} + w_{L\perp})/{\rm D_{Feq}}$ or

$${\rm D_{Feq}} = \pi\left(w_{L//} w_{L\perp}\right)/\lambda = \left[{\rm D}_{F\perp}{\rm D}_{F//}\right]^{1/2} \quad (17')$$

that is, just the Fresnel equivalent distance.

C. C-Factor and SMI Waveform

Using (5) with $\alpha = 5$, we have

$$\mathrm{C} = 3.06\eta_E \mathrm{D}/n_c l_c. \tag{18}$$

Letting in (18) the η_E values of (11) and (13), we get for the NF and FF

$$\mathrm{C_{NF}} = 2.17(w_L \mathrm{D}/\mathrm{D}_F)/n_c l_c \quad \mathrm{C_{FF}} = 2.17\ w_L/n_c l_c. \tag{19}$$

From (19), we see that C increases with distance D in the NF and becomes independent of distance in the FF. At the Fresnel distance $\mathrm{D} = \mathrm{D}_F$, it is $\mathrm{C_{NF}} = \mathrm{C_{FF}}$.

For an elliptical spot, (19) still applies by changing the factor w_L into w_{Leq} and D_F into $\mathrm{D_{Feq}}$ as indicated by (17) and (17').

D. Linewidth

The linewidth of the diode laser is noticeably affected by optical feedback at the medium/high levels corresponding to regions II and III of the Tkach and Chraplyvy diagram [11], [17]. The effect of feedback has been studied by Schunk and Petermann [18] and by Laurent et al. [19]. They found that the ratio of perturbed $\Delta\nu_{\mathrm{SMI}}$ to unperturbed $\Delta\nu_0$ linewidth is given by

$$\Delta\nu_{\mathrm{SMI}}/\Delta\nu_0 = 1/(1+\mathrm{C})^2. \tag{20}$$

The maximum operative distance covered by the SMI measurement is limited by the coherence length L_c of the source. In the common case of a laser with a Lorentzian distribution of linewidth, L_c is found as [16]

$$L_c = c/\pi\Delta\nu \tag{21}$$

where $\Delta\nu$ is the full-width at half-maximum (FWHM) of the frequency distribution.

For a Gaussian linewidth, the right-hand term in (21) shall be multiplied by 1.38, and similar factors, all close to one, are found [16] for a different choice of the $\Delta\nu$ metric.

The decrease of SMI signal AM when the pathlength $L =$ 2-D of operation becomes comparable to L_c is found, for a Lorentzian linewidth, as [16]

$$I_{\mathrm{PD}}(\mathrm{D})/I_{\mathrm{PD}}(0) = \exp -(2\mathrm{D}/L_c) \tag{22}$$

whereas, in the case of a Gaussian distribution, it is given by

$$I_{\mathrm{PD}}(\mathrm{D})/I_{\mathrm{PD}}(0) = \exp -(2\mathrm{D})^2/2L_c^2. \tag{22'}$$

Last, in view of (20) and (21), the coherence length depends on the C factor as follows:

$$L_c = L_{c0}(1+C)^2 \tag{23}$$

where L_{c0} being the value of the unperturbed coherence length.

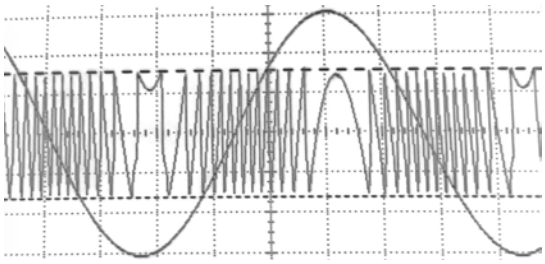

Fig. 3. Measured SMI waveform obtained with a sine wave drive (≈20-μm peak-to-peak, 30 Hz) of the loudspeaker target (white paper diffusing surface) at 20-cm stand-off distance. Laser diode is WSLM-1550-015 at 8.1 mW. Vertical scale of SMI signal AM is 200 mV/div and time scale 5 ms/div.

III. Experimental Validation

We have used the general-purpose DFB diode laser WSLM-1550-015m-K of wave spectra. The laser has a measured threshold $I_{\mathrm{bias}} = 5$ mA (half the value of manufacturer's specs) and emits up to 15 mW at $\lambda = 1500$ nm with a slope efficiency of 0.324 mW/mA (almost double the value of specs). We used it at $I_{\mathrm{bias}} = 30$-mA and 8.1-mW power. The unit comes in a collimating tube with an aspheric objective lens (4.5-mm aperture diameter, 0.4 NA) yielding a beam of 1-mrad divergence and with 3 × 1.5 mm diameters (corresponding to $\mathrm{w}_{//} =$ 0.75 mm and $\mathrm{w}_{\perp} = 0.375$ mm, see Section III-E).

The monitor photodiode incorporated in the package yields a current $\sigma_{\mathrm{ph}}\mathrm{P}_0 = 560\ \mu$A at 8.1-mW front-exit power and was connected to a $R_F = 27$-kΩ transimpedance preamp built with a TL-081op amp, followed by a G = 16 gain stage, for a total equivalent transresistance of $R_{\mathrm{Feq}} = R_F\ \mathrm{G} = 432$ kΩ.

The emitted beam was sent directly onto a loudspeaker cone covered by plain white paper to work as a noncooperative target. Feeding the loudspeaker with a sine wave drive signal $\mathrm{D}_0\cos\omega\mathrm{t}$, we observed the typical SMI waveforms, that is, $I_{\mathrm{PD}} = I_{\mathrm{PD0}}\cos(2\mathrm{k}\mathrm{D}_0\cos\omega\mathrm{t})$, as illustrated in Fig. 3. Here, by counting $N = 26$ SMI fringes in a period, we can tell the peak-to-peak AM of the vibration is $\mathrm{N}(\lambda/2) = 20.1\ \mu$m.

We have measured AM $V_{\mathrm{PD}} = R_{\mathrm{Feq}}I_{\mathrm{PD}}$ of the SMI voltage signal (at the output of the op-amp preampl) at several distances, and with a diffusive target, a piece of white paper glued on the loudspeaker cone.

Due to the speckle-pattern statistics [3], the AM of the SMI signal was observed to change from point to point of the target and vary in a typical range indicated by the relatively large uncertainty bars of the experimental values reported in Fig. 4. The expected output signal (peak value) in the NF is from (15)

$$V_{\mathrm{out}} = R_{\mathrm{Feq}}I_{\mathrm{PD}} = R_{\mathrm{Feq}}0.425(\sigma_{\mathrm{PD}}P_0)(w_L/\mathrm{D}_F)$$

which, by inserting the values found above, gives: $V_{\mathrm{out}} =$ 101.5 mV (peak value) that becomes 203 mV as peak-to-peak value, in good match to the 200 mV found experimentally at $\mathrm{D} < \mathrm{D}_F$ (Fig. 4).

Signal is also corrupted by noise and disturbances. Basically, the noise background is given by two contributions: 1) shot noise of the local oscillator and 2) microphonic (or acoustic) disturbances collected from the ambient. Shot noise, expressed in terms of detected current $I_0 = \sigma_{\mathrm{PD}}P_0$, is given by

$$i_n = (2e\ I_0\ B)^{1/2}. \tag{24}$$

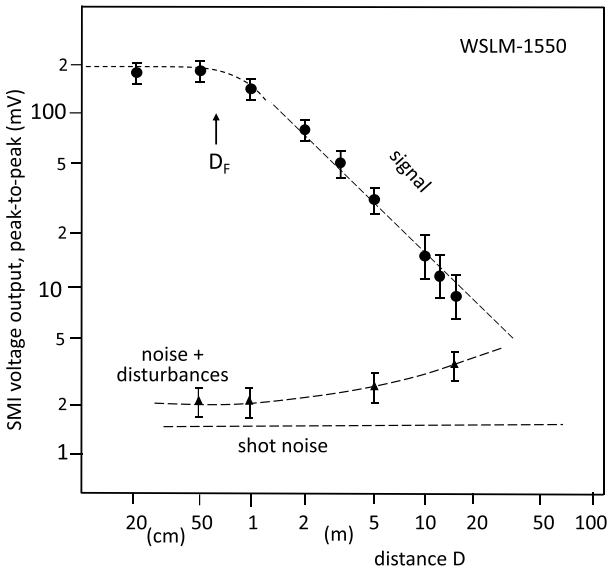

Fig. 4. Measured SMI signal voltage (peak-to-peak) at the preamp output versus distance for the WSLM-1550-015m-K at 8.1 mW and $R_{Feqv} = 432$ kΩ, target white plain paper, objective is the original collimating lens (4.5-mm aperture diameter, 0.4 NA). The trend as D^{-1} of (6) is well matched, and also, the saturation below the Fresnel distance is observed. The waveform is clean till $D = 12$ m, at which the SNR = 3.6. At SNR = 1, the reach is around 40 m in conditions of disturbance collected from a normal lab ambient but could exceed 100 m in the limit of shot noise of returning power.

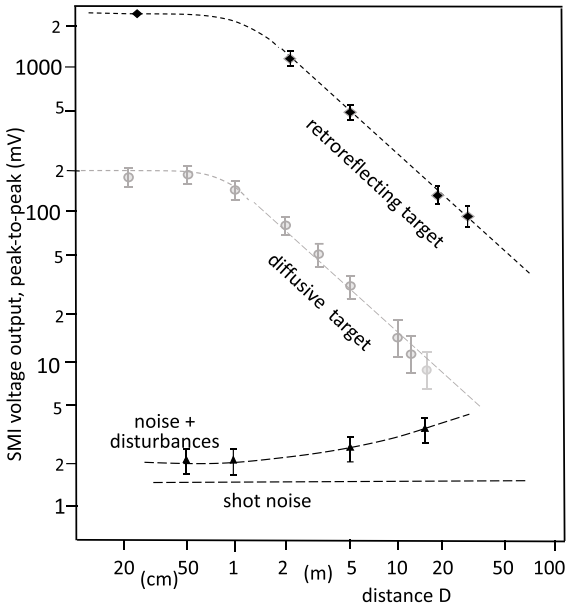

Fig. 5. SMI signal voltage (peak-to-peak) versus distance for the WSLM-1550-015m-K laser with the original collimating lens (4.5 mm diameter, 0.4 NA). The retroreflective target SMI AM is ≈18 times larger than the signal from a diffusive target.

Assuming $B = 10$ kHz for the TL-081 preamp and being $I_0 = \sigma_{PD} P_0 = 560$ μA (measured value), the rms current noise is $i_n = 1.33$ nA, and the voltage output noise is $R_{Feq} i_n = 0.532$ mV rms that becomes ≈1.6 mV as peak-to-peak value.

Disturbances are due to the microphonics or stray vibrations that the setup collects from the ambient. They have a spectral distribution decreasing with frequency [20]. To reduce microphonics, we have introduced a single-zero *RC* high-pass filter at the op-amp preamp output, with a frequency cutoff $f_1 = 80$ Hz, which significantly decreases the disturbance (of a factor about 30), bringing the total noise background at a few millivolts.

In Fig. 4, we plot the results of measurements of SMI signal AM V_{out} versus distance D, along with the noise contributions.

The trend of experimental data is in full agreement with that predicted by (16). SMI signal has a nearly constant AM in the NF ($D < D_F$) and a 1/D trend in the FF ($D > D_F$).

Again, the break point (crossing of the straight lines of the NF and FF) is the Fresnel distance that in Fig. 4 can be read as $D_F \approx 0.6$ m (with an uncertainty of ±0.1 m), in accordance with the value 0.57 m calculated by (17).

At D = 12 m, the penultimate point in Fig. 4, we obtained a fairly good SMI waveform, with SNR = 3.6, still adequate to carry a vibrometer signal or allow a λ/2 fringe-counting displacement measurement. At D = 15 m, the SMI signal was frequently corrupted by disturbances and had a too poor SNR (≈1.8) to make measurements. Yet, the limit at SNR = 1 for the total noise background is $D_{tot,n} \approx 40$ m. If microphonic disturbance was eliminated and the sole shot noise remains, the range could potentially reach $D_{shot,n} = 110$ m.

A similar finding was reported in [15] for the HL7851G diode laser, with D = 10 m as the maximum operative distance for a good SMI signal and 20 m as the distance of barely visible SMI signal.

The signal-to-noise ratio (SNR) of the SMI signal AM is simply given by the difference in the log scale of Fig. 4, of AM to total background, that we can read as 100 (or 40 dB) in the NF and that decreases by 20 dB/decade in the FF starting from the Fresnel distance D_F onward. In our setup, if the microphonic disturbance could be removed, the SNR increases of ≈3 dB.

Another important observation is the distance $D_{C=1}$ at which the *switching* in the SMI waveform takes places, indicative of the C = 1 condition. We measured $D_{C=1} = 25$ cm (with an uncertainty of ±5 cm). From the D/D_F dependence (19), at the Fresnel distance we get the C in the FF, $C_F = 0.57/0.25 = 2.34$, a value used later in Section III-G.

A. α-Factor

We have used the graphical method described in [8] (see also Figs. 5–43 on [3, p. 222]) and it was found consistently $\alpha = 5$ (±0.3).

B. Operation on a Retroreflective Target

Results reported in previous sections are for a *diffusive* target of which we want to measure displacement or vibrations. Using a *retroreflective* surface as a target, we can increase the returning power of the retroreflective gain G (defined as the radiance ratio) and the SMI signal AM of a factor $G^{1/2}$(because of the coherent detection). For a typical retroreflective tape (EG 3430 of 3M[1], the response coefficient is specified as $\rho = 120$ cd/lm, and therefore, respect to the ideal diffusive target (which has $\rho_{diff} = \pi^{-1}$cd/lm), the retroreflective gain is $G = \pi\rho = 377$ in radiant power and $G^{1/2} = 19.4$ in SMI signal AM.

[1]Trademarked.

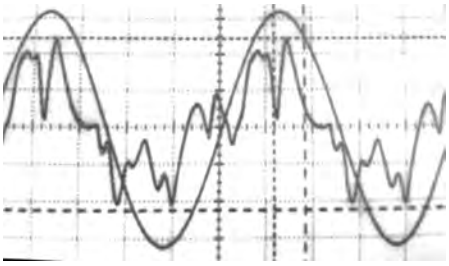

Fig. 6. Small misalignments of the retroreflective surface (EG 3430 3M[1]) normal respect to illumination/observation directions makes the SMI signal become the composite of the normal fringe signal cos 2kS(t) plus that of the driving signal S(t), here a sinusoid. Distance is 15 m, AMs: fringe signal ≈ 200 mV (peak-to-peak) and S(t) component ≈ 600 mV (peak-to-peak).

Of course, the improvement of levels is paid by the constraint of invasiveness, because we shall apply the retroreflective tape (or varnish) to the target under measurement.

Second and less known, we shall also align the angles of the illumination beamα and of the observation direction β so as to coincide with the target surface normal, because gain G is a decreasing function of the deviations α and β from the normal.

We have measured the SMI signal AM for a target covered by the EG 3430 retroreflective tape, and the results are reported in Fig. 5. The radiation diagram of the retroreflective tape had a (measured) width (HWHM) of 0.05 rad (3°), a value compatible with a response coefficient of 120 cd/lm, and the measured gain of SMI signal AM is 18 (±1), consistent with specifications.

The illumination and observation angles are equal ($\alpha = \beta$) in the SMI operation, and it was found that even a small misalignment like $\alpha = \beta = 0.5°$ seriously alters the SMI waveform. Indeed, working on the tail of the radiation pattern of the retroreflective surface introduces an artifact: the small change of α and β due to parallax, while the target distance S(t) changes, drags a small replica of S(t) to the fringes signal cos 2kS(t) of the SMI, as shown in the exemplary waveform of Fig. 6.

Additional to the invasiveness, another drawback of using the retroreflecting target is the increase of C by a factor $G^{1/2}$, which brings about a distortion of the SMI signal waveform and eventually entering in the coherence collapse region [3], [9], [17].

C. Sweeping the Laser

A well-known method of absolute distance measurement by a λ-sweep [1], [3], [21] consists in applying a linear sweep ΔI_b to the drive current of the laser diode (Fig. 7), so as to obtain a wavelength change $\Delta\lambda = \alpha_\lambda \Delta I_b$ and hence a phase signal $\Delta\Phi = 2\Delta kD = 4\pi(\Delta\lambda/\lambda^2)D$ variation. Thus, an SMI signal is obtained on a stationary target at distance D. By counting the 2π-periods of $\Delta\Phi$, we obtain the distance as a number $N = \Delta\Phi/2\pi = D/(\lambda^2/2\Delta\lambda)$ in units $D_0 = \lambda^2/2\Delta\lambda$ [1], [3], [24].

We used a ΔI_b = 0.3–0.8 mA to demonstrate a D_0 = 20- to 50-cm resolution (for automotive LiDAR application) on a distance D = 5–20-m.

An exemplary waveform obtained at D = 12 m with the WLSM-1550 at 8.1 mW is shown in Fig. 7.

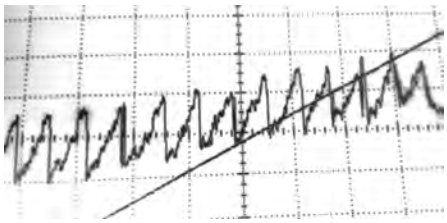

Fig. 7. Triangular wave (frequency 80 Hz) drives the bias current with a ramp signal ΔI_b = 0.8 mA generating a λ-sweep of 2.5 pm and a number N (24 in total, a portion of which is shown here) of SMI periods, each representing a D_0 = 50-cm count of the target distance D = 12 m. Diode laser is WSLM-1550-015m-K at 8.1 mW, SNR ≈ 4, target is white paper. Vertical scale 20 mV/div and horizontal scale 5 ms/div.

D. Linewidth and Coherence Length

We have measured the WSLM-1550-015 linewidth by means of the fiber Mach–Zehnder interferometer HP 11 980 A instrument, connected to an HP 83 810 A signal analyzer to realize a self-homodyne linewidth measurement [22]. We obtained $\Delta\nu$ = 5.1 MHz, corresponding to a coherence length for the unperturbed laser (21), of L_c = 19.4 m. This value implies, according to (22), an SMI signal AM reduced to 1/e at a distance $2D_{1/e} = L_c$ or $D_{1/e}$ = 9.7 m. At increasing distance, L_c increases from (23) as $(1 + C)^2$, or almost quadratically with C, up to the value $(1 + C_F)^2$ = 11.1 at the Fresnel distance D_F = 0.57 m [(9)] onward, so that $2D_{1/e} = L_c$ is for $D_{1/e}$ = 107 m. Thus, we can conclude that coherence length in our SMI experiment is large enough to make negligible the AM loss due to coherence effects.

E. Spot Size

The spot size of the beam on the target is an important parameter, which establishes the sampling (or pixel) size of the scene of which we are measuring the distance.

From the rule of propagation of a circular Gaussian beam [23], the spot size w_T increases with distance D as the quadratic sum of the initial spot size w_G and of the divergence term, i.e.,

$$w_T^2 = w_G^2 + (\lambda/\pi w_G)^2 D^2 \tag{25}$$

where w_G is the spot size of the beam leaving the collimating optics—i.e., the objective lens in Fig. 1. As already mentioned, the lens radius w_L shall be chosen larger than the spot size to transmit and collect all the laser power. Anyway, all the considerations developed below are valid for the spot size w_T irrespective of the w_L value.

The manufacturer usually specifies the diameter d spot size, i.e., a quantity identified as the D4Σ of the power distribution across the beam according to the standard [24], and gives the diameters $d_{//}$ and $d_\perp$ in the directions parallel and perpendicular to the junction.

However, in our calculations, we have used the rms or standard deviation w of the distribution. The relation to the full-width D4Σ (or FW4σ) to the Gaussian spot size w (either w_G or w_T) is

$$\mathrm{FW4}\sigma = 4w. \tag{26}$$

For the WSLM-1550-015 laser, the diameter spot sizes are specified as $d_{//}$ = 3 mm and $d_\perp$ = 1.5 mm, and the measurement at the focusing lens output confirmed these values. For

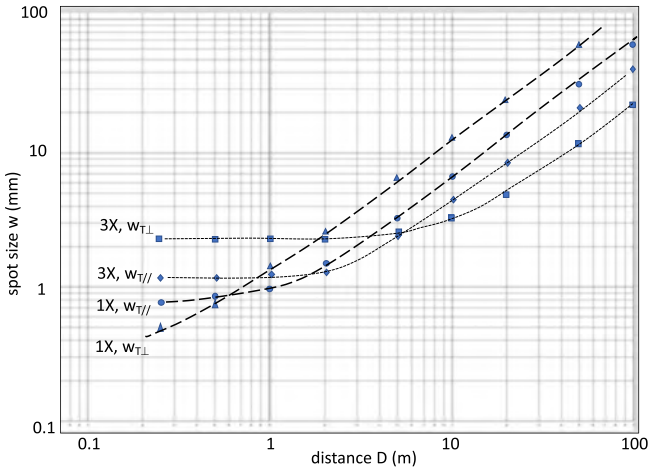

Fig. 8. Spot size $w_{T//}$ and $w_{T\perp}$(all rms values, for the full-width D4Σ multiply by 4) as a function of distance D. Starting values are $w_{T//} = 0.75$ mm and $w_{T\perp} = 0.375$. mm for the built-in objective of 4.5 mm dia., 0.4 NA. Points labeled 3X are for a beam expander magnifying the beam by 3, which makes the increase of w_T with distance slower.

these diameters (FWHM values), the corresponding radius spot sizes (rms value of the Gaussian) are: $w_{//} = d_{//}/4 = 0.75$ mm and $w_\perp = w_{\text{Leq}} = 0.56$ mm.

As (25) applies separately to $w_{T//}$ and $w_{T\perp}$, we have different behaviors of the size along the axes // and $\perp$ to the junction. The // and $\perp$ divergences are $\theta_\perp = \lambda/\pi w_\perp = 1.316$ mrad and $\theta_{//} = \lambda/\pi w_{//} = 0.658$ mrad, and thus, the elliptical beam starts with the major axis along the // direction for short distances and becomes along the $\perp$ axis for long distances, passing through a circular shape at a distance found, for a Gaussian mode, as $D_{\text{Feq}} = \pi w_{//} w_\perp/\lambda = 0.57$ m—the equivalent Fresnel distance (measured distance was 50 ± 5 cm).

From (25), we can calculate the D4Σ spot sizes $w_{T//}$ and $w_{T\perp}$ at some target distances, e.g., D = 1, 10 and 50 m, and we find these pairs for the diameters $d_{T//} = 4w_{T//}$ and $d_{T\perp} = 4w_{T\perp}$: (3.96, 5.47), (26.5, 52), and (131, 262) all in mm. The trend of spot sizes $w_{T//}$ and $w_{T\perp}$ with distance D is plotted in Fig. 8.

IV. Discussion

A. Indirect Measurements of Laser and SMI Parameters

Interesting to note, the measurements carried out with the simple SMI optical setup of Fig. 1 allow us to trace back several parameters of the experiment and of the laser.

By measuring the distance $D_{C=1}$ at which C = 1 from the onset of a switching in the SMI waveform (Fig. 2), we can get C at all distances. Indeed, using (19), we have: $C = D/D_{C=1}$ for $D < D_{\text{Feq}}$ and $C = D_{\text{Feq}}/dc_{=1}$, for $D \geq D_{\text{Feq}}$. This method is much simpler than those currently used [3], based on the measurements of time intervals of waveform details.

By measuring the Fresnel distance D_{Feq}, as the intersection of the asymptotic lines of the NF and FF in Fig. 3, we can trace back (17) the effective beam size as $w_{\text{Leq}} = \sqrt{(\lambda D_{\text{Feq}}/\pi)}$.

Inserting $D_{c=1} = 25$ cm in (19), along with $w_{\text{Leq}} = 0.56$ mm and $n_c = 3.5$, we can solve for the cavity length and obtain the estimate $l_c = 150$ μm. This is a new method to estimate the cavity length, supplementing the current practice based on the free spectral range [25].

With the FF C (=C_{Feq}, at $D > D_{\text{Feq}}$) and the value $\Delta\nu_{\text{SMI(FF)}}$ at $D \geq D_F$, we may calculate the unperturbed linewidth of the laser source, using (20), and get $\Delta\nu_0 = \Delta\nu_{\text{SMI(FF)}}(1 + C_{\text{Feq}})^2$.

Last, by measuring the loss in signal AM due to decreased coherence at large distances, $A_L = I_{\text{PD}}(D)/I_{\text{PD}}/(0)$, we may: 1) trace back [(22)] the coherence length as $L_c = 2\text{-}D/(\ln A_L^{-1})$ for the Lorentzian case—or $L_c = D(2/\ln A_L^{-1})^{1/2}$ for the Gaussian case; 2) from the exponential decay with D; and 3) whether data fit better the $-D/L_c$ or $-(D/L_c)^2$ trend, we may determine whether the laser line has a Lorentzian or Gaussian distribution that indicates, respectively, the prevalence of collision or Doppler effect as the line-broadening mechanism.

B. Hints for Performance Improvement

By increasing the laser emitted power of a factor F, the SMI signal AM increases of $\sqrt{F}$ and the shot noise of $\sqrt{F}$, so their ratio as well their intercept at SNR = 1 remains at the same distance (but advantageously, the relative weight of disturbances respect to shot noise is reduced by a factor $\sqrt{F}$, and linewidth is decreased by F [26]).

Better if we use a collimating telescope (inserted after the lens in Fig. 1) with (linear) magnification M of the spot size, that increases the power collection by M^2; thus, both signal and shot noise increase of M. As w_G now becomes Mw_G, the Fresnel distance is increased by M^2[(2)] and, useful to have, the SNR = 1 range increases of a factor M. Same useful, the spot size increases less sharply with distance: for example, for $M = 3$, at 1, 10, and 50 m, the pairs of $d_{T//}$ and d_T are (9.04, 4.48), (39.4, 18.1), and (44.8, 87.6), as plotted in Fig. 8.

Also useful is using the balanced readout of the SMI signal [27], which can increase the SNR and the covered range of a factor up to 8 dB.

Finally, to improve the limit of coherence-loss-related range, in addition to exploit the inverse-power dependence of linewidth [26], a diode laser with larger cavity length is preferable, so as to increase the Q-factor (or selectivity) of the cavity resonator.

V. Conclusion

We have derived, for the first time to the best of our knowledge, the fundamental theory of SMI quantities (signal AM and SNR, C factor, and linewidth) versus distance, valid also for an elliptical-beam propagation. The results we present are the base for designing measurement applications, such as long standoff distance vibration sensing, displacements and distance/velocity measurement, and LiDAR. The theory indicates that the SMI signal AM is constant up to the Fresnel distance of the objective lens and then rolls off with the inverse distance (specific of the coherent detection), with an SNR up to 40 dB in the NF.

The experimental validation performed with a commercial DFB diode laser at 1550 nm nicely confirms the theory and is itself a simple prototype working up to 12-m distance with the original, small collimating lens (4.5-mm aperture diameter, 0.4 NA) of the laser, and on a plain diffuser at the target receiving surface. The use of a retroreflective target was found

problematic not only for its invasiveness, but also because an angular alignment is required to avoid artifacts.

REFERENCES

[1] S. Donati, "Developing self-mixing interferometry for instrumentation and measurements," *Laser Photon. Rev.*, vol. 6, no. 3, pp. 393–417, May 2012, doi: 10.1002/lpor.201100002.

[2] T. Taimre, M. Nikolić, K. Bertling, Y. L. Lim, T. Bosch, and A. D. Rakić, "Laser feedback interferometry: A tutorial on the self-mixing effect for coherent sensing," *Adv. Opt. Photon.*, vol. 7, no. 3, pp. 570–631, Sep. 2015.

[3] S. Donati, *Photonic Instrumentation*, 2nd ed., Boca Raton, FL, USA: CRC Press, 2023, ch. 5.

[4] S. Donati, "Vibration measurements by self-mixing interferometry: An overview of configurations and benchmark performances," *Vibration*, vol. 6, no. 3, pp. 625–644, Aug. 2023.

[5] S. Donati and M. Norgia, "Self-mixing interferometer with a laser diode: Unveiling the FM channel and its advantages respect to the AM channel," *IEEE J. Quantum Electron.*, vol. 53, no. 5, pp. 1–10, Oct. 2017.

[6] E. M. Randone and S. Donati, "Self-mixing interferometer: Analysis of the output signals," *Opt. Exp.*, vol. 14, no. 20, pp. 9188–9196, 2006.

[7] S. Donati, *Photodetectors—Devices, Circuits and Applications*, 2nd ed., Hoboken, NJ, USA: Wiley, 2021.

[8] Y. Yu, G. Giuliani, and S. Donati, "Measurement of the linewidth enhancement factor of semiconductor lasers based on the optical feedback self-mixing effect," *IEEE Photon. Technol. Lett.*, vol. 16, no. 4, pp. 990–992, Apr. 2004.

[9] S. Donati and C. Mirasso, "Optical chaotic cryptography," *IEEE J. Quantum Electron.*, vol. 38, pp. 1138–1184, Sep. 2002.

[10] S. Donati and S.-K. Hwang, "Chaos and high-level dynamics in coupled lasers and their applications," *Prog. Quantum Electron.*, vol. 36, nos. 2–3, pp. 293–341, Mar. 2012.

[11] R. W. Tkach and A. R. Chraplyvy, "Regimes of feedback effects in 1.5-μm distributed feedback laser," *J. Lightw. Technol.*, vol. 4, no. 11, pp. 1655–1661, Nov. 1986.

[12] C. V. Poulton et al., "Coherent solid-state LiDAR with silicon photonic optical phased arrays," *Opt. Lett.*, vol. 42, no. 20, pp. 4091–4094, Oct. 2017.

[13] T.-Y. Chung, R.-R. Chang, and Y.-H. Chen, "Demonstration of FMCW LiDAR using a diode laser feedback with PQ: PMMA VBG," *OSA Continuum*, vol. 4, no. 10, p. 2687, Oct. 2021.

[14] Y. Wang et al., "Laser feedback frequency-modulated continuous-wave LiDAR and 3-D imaging," *IEEE Trans. Instrum. Meas.*, vol. 72, pp. 1–9, 2023.

[15] A. Magnani, A. Pesatori, and M. Norgia, "Real-time self-mixing interferometer for long distances," *IEEE Trans. Instrum. Meas.*, vol. 63, no. 7, pp. 1804–1809, Jul. 2014.

[16] C. Akcay, P. Perrin, and J. P. Rolland, "Estimation of longitudinal resolution in optical coherence imaging," *Appl. Opt.*, vol. 41, no. 25, pp. 5256–5262, 2002.

[17] S. Donati and R.-H. Horng, "The diagram of feedback regimes revisited," *IEEE J. Sel. Topics Quantum Electron.*, vol. 19, no. 4, Jul. 2013, Art. no. 1500309, doi: 10.1109/JSTQE.2012.2234445.

[18] N. Schunk and K. Petermann, "Numerical analysis of the feedback regimes for a single-mode semiconductor laser with external feedback," *IEEE J. Quantum Electron.*, vol. 24, no. 7, pp. 1242–1247, Jul. 1988.

[19] P. Laurent, A. Clairon, and C. Breant, "Frequency noise analysis of optically self-locked diode lasers," *IEEE J. Quantum Electron.*, vol. 25, no. 6, pp. 1131–1142, Jun. 1989.

[20] S. Donati, G. Martini, and S.-K. Hwang, "Measurement of ambient vibration by self-mixing interferometry and its application to intrusion detection," *Opt. Eng.*, vol. 57, no. 5, Apr. 2018, Art. no. 051508, doi: 10.1117/1.oe.57.5.051508.

[21] M. Norgia, G. Giuliani, and S. Donati, "Absolute distance measurement with improved accuracy using laser diode self-mixing interferometry in a closed loop," *IEEE Trans. Instrum. Meas.*, vol. 56, no. 5, pp. 1894–1900, Oct. 2007.

[22] H. Ludvigsen, M. Tossavainen, and M. Kaivola, "Laser linewidth measurements using self-homodyne detection with short delay," *Opt. Commun.*, vol. 155, nos. 1–3, pp. 180–186, Oct. 1998.

[23] *See Ref [3], Sect.2.1.*

[24] *Test Methods for Laser Beam Widths, Divergence Angles and Beam Propagation Ratios*, ISO Standard 11146-1:2021, 2021.

[25] A. Staley et al., "High precision optical cavity length and width measurements using double modulation," *Opt. Exp.*, vol. 23, no. 15, pp. 19417–19431, 2015.

[26] *See Ref.[5], Eq.13.*

[27] P. Esmaili, M. Norgia, and S. Donati, "Noise decrease in a balanced self-mixing interferometer: Theory and experiments," *IEEE Trans. Instrum. Meas.*, vol. 72, pp. 1–8, 2023.

Alfred Albert was born in Jakarta, Indonesia, in August 1993. He received the M.Sc. degree in electronics and computer engineering from the National Taiwan University of Science and Technology (NTUST), Taipei, Taiwan, in 2018, where he is currently pursuing the Ph.D. degree in electronics and computer engineering.

His research interests include nanophotonics and diode laser interferometry.

Silvano Donati (Life Fellow, IEEE) has been a Full Professor of University of Pavia, Pavia, Italy, since 1980 and became Emeritus in 2015. He has authored or co-authored 350+ papers, holds a dozen patents, and has written two books, "Photodetectors" 2nd ed., IEEE Wiley 2021 and "Photonic Instrumentation" 2nd ed., CRC 2023, covering the subject of his courses. His main achievements have been self-mixing interferometry and chaos-shift-keying cryptography, the topics covered in his Distinguished Lecture talk given in 21 LEOS (now IPS) Chapters in two terms (2007–2009) and continued as a Traveling Lecturer of OSA (now Optica) and SPIE on Self-Mixing and Lidars to date, covering a total 105 Chapters visited.

Mr. Donati has received several awards from the AEIT and IEEE, in particular, the Marconi medal, the Aaron Kressel Award, and the Distinguished Service Award of the IEEE Photonics Society. He was the founder (1996) and first Chairperson (1997–2001) of the Italian LEOS Chapter, LEOS VP Region 8 Membership (2002–2004), and BoG (2004–2006), and the Chairperson of the IEEE Italy Section (2008–2009). He has spent semesters as Visiting Professor in the Universities of Taiwan: NTU, NSYSU, NCKU, NCHU, NTUT, and presently NTUST/ HiSiPIC.

San-Liang Lee (Senior Member, IEEE) received the Ph.D. degree in electrical and computer engineering from the University of California, Santa Barbara (UCSB), Santa Barbara, CA, USA, in 1995.

He joined the faculty of the Department of Electronic and Computer Engineering, National Taiwan University of Science and Technology (NTUST), Taipei, Taiwan, in 1988, and became a Full Professor in 2002 and a Chair Professor in 2019. He was the Vice President of the University, from 2011 to 2014. He served as the Dean of Academic Affairs Office and the Chairperson of the Department of Electronic and Computer Engineering for 2005–2008. He was the Director of the research program on Silicon Photonics and Integrated Circuits sponsored by the National Science and Technology Council (NSTC), Taiwan, from 2018 to 2023. He was also the Director of Photonic Division, Department of Engineering and Technologies, NSTC, from 2021 to 2023. He is the founding Dean of Industry-Academia Innovation College, NTUST, since 2022. He was a Visiting Scientist at Massachusetts Institute of Technology (MIT), from 2010 to 2011. He has published more than 250 referred papers in international journals and conferences and holds >30 patents. His research interests include semiconductor optoelectronic components, photonic integrated circuits, nanophotonics, and optical networking technologies.

Dr. Lee received the 2018 Outstanding Research Award from NSTC and 2019 MOC Contribution Award from the Microoptics Group of Japanese Society of Applied Physics. He served as the Electronic Section Editor of the SCI indexed Journal and Journal of the Chinese Institute of Engineers from 2007 to 2012. Since 2013, he has been serving as the Associate Editor of IEEE Access Journal.